Geosci. Model Dev., 10, 1607–1620, 2017
www.geosci-model-dev.net/10/1607/2017/
doi:10.5194/gmd-10-1607-2017

Geoscientific Model Development
Open Access
EGU

Development of a new gas-flaring emission dataset for southern West Africa

Konrad Deetz and Bernhard Vogel

Institute of Meteorology and Climate Research, Karlsruhe Institute of Technology (KIT), Karlsruhe, Germany

Correspondence to: Konrad Deetz (konrad.deetz@kit.edu)

Received: 4 May 2016 – Discussion started: 1 August 2016
Revised: 13 March 2017 – Accepted: 21 March 2017 – Published: 18 April 2017

Abstract. A new gas-flaring emission parameterization has been developed, which combines remote sensing observations using Visible Infrared Imaging Radiometer Suite (VIIRS) nighttime data with combustion equations. The parameterization has been applied to southern West Africa, including the Niger Delta as a region that is highly exposed to gas flaring. Two 2-month datasets for June–July 2014 and 2015 were created. The parameterization delivers emissions of CO, CO_2, NO, NO_2 and SO_2. A flaring climatology for both time periods has been derived. The uncertainties owing to cloud cover, parameter selection, natural gas composition and the interannual differences are assessed. The largest uncertainties in the emission estimation are linked to the parameter selection. It can be shown that the flaring emissions in Nigeria have significantly decreased by 25 % from 2014 to 2015. Existing emission inventories were used for validation. CO_2 emissions with the estimated uncertainty in parentheses of 2.7 (3.6/0.5) Tg yr^{-1} for 2014 and 2.0 (2.7/0.4) Tg yr^{-1} for 2015 were derived. Regarding the uncertainty range, the emission estimate is in the same order of magnitude compared to existing emission inventories with a tendency for underestimation. The deviations might be attributed to a shortage in information about the combustion efficiency within southern West Africa, the decreasing trend in gas flaring or inconsistent emission sector definitions. The parameterization source code is available as a package of R scripts.

1 Introduction

Gas flaring is a globally used method to dispose flammable, toxic or corrosive vapors to less reactive compounds at oil production sites and refineries. In regions of insufficient transportation infrastructure or missing consumers, flaring is also commonly applied.

CDIAC (2015a) estimated the global gas-flaring emission of carbon dioxide to 267.7 million tons (0.83 % of total emissions) in 2008. Flaring and venting of gas significantly contributes to greenhouse gas emissions and therefore to global climate change. The five countries with the highest flaring amounts in billion cubic meters (bcm) are Russia (35), Nigeria (15), Iran (10), Iraq (10) and USA (5) (Elvidge et al., 2016). These estimates were produced by National Oceanic and Atmospheric Administration (NOAA) using Defense Meteorological Satellite Program (DMSP) remote sensing data. Preliminary updates in global flaring estimates from NOAA for 2013 and 2014 are available at http://ngdc.noaa.gov/eog/viirs/download_global_flare.html.

Recently, especially with the development of remote sensing observation techniques (e.g., Elvidge et al., 1997, 2013), emissions from gas flaring moved into focus for atmospheric research involving the efforts of reducing pollution and waste of resources. The World Bank led the initiatives "Global Gas Flaring Reduction Partnership" and "Zero Routine Flaring by 2030" to promote the efficient use of flare gas.

Instead of relying on national statistics of gas production and consumption for estimating the flaring amount, remote sensing techniques can estimate the flaring amount directly via multispectral data (Elvidge et al., 2013). Elvidge et al. (2009) developed a 15-year dataset of global and national gas-flaring efficiency from 1994 to 2008 by using data from DMSP. Elvidge et al. (2015) presented methods to de-

rive global surveys of natural gas flaring using DMSP. For 2012 they have identified 7467 flares globally, with an estimated volume of flared gas of 143 (±13.6) bcm. Doumbia et al. (2014) combined DMSP with emission factors for flaring, to estimate the flaring emissions for southern West Africa (SWA). The satellite product Visible Infrared Imaging Radiometer Suite (VIIRS) Nightfire (Elvidge et al., 2013), which is freely available as "VIIRS Nightfire Nighttime Detection and Characterization of Combustion Sources" (VIIRS, 2015a) (VNF hereafter), is now the most widely used product to derive flaring emissions from satellite imagery. By using VNF, Zhang et al. (2015) estimated the methane consumption and the release of CO_2 from gas flaring for the northern USA, which agreed with field data within an uncertainty range of ±50 %.

Also in the second largest flaring country Nigeria, the awareness of gas flaring has increased. Nigeria shows the fourth highest number of flare sites (approx. 300) worldwide after USA, Russia and Canada (Elvidge et al., 2015). On gasflaretracker.ng the attention of the government, industry and society is called to the flaring problem by interactive maps of flare infrastructure, amounts and costs. The implications of gas flaring in Nigeria are far reaching. It influences the environment by noise and deterioration of the air quality (Osuji and Avwiri, 2005). Nwankwo and Ogagarue (2011) have measured higher concentrations of heavy metals in surface water of a gas-flared environment in Delta State, Nigeria. Adverse ecological and bacterial spectrum modifications by gas flaring are indicated by Nwaugo et al. (2006). Gas flaring also causes acid rain, which causes economic burden via rapid corrosion of zinc roofs (Ekpoh and Obia, 2010) and causes retardation in crop growth owing to high temperatures (Dung et al., 2008).

The project DACCIWA (Dynamics–aerosol–chemistry–cloud interactions in West Africa; Knippertz et al., 2015) investigates the influence of anthropogenic and natural emissions on the atmospheric composition over SWA, including the flaring hotspot Nigeria, to quantify the effects on meteorology and cloud characteristics. To consider the SWA gas-flaring emissions (e.g., in an atmospheric model), this study presents a method to derive emission fluxes by combining the state-of-the-art flaring detection VNF and the combustion equations of Ismail and Umukoro (2014), which does not use emission factors. The new parameterization is robust and easy to apply to new research questions according to flexibility in the spatiotemporal resolution.

The parameterization is presented in Sect. 2. Results of the application to SWA, including the spatial distribution of gas flaring, the emission estimation and the uncertainty assessment are investigated in Sect. 3. Section 4 places the emission estimates in the context of existing inventories. The results are summarized and discussed in Sect. 5.

2 Parameterization of gas-flaring emissions

The new parameterization for gas flaring presented here, is based on VNF and the combustion equations of Ismail and Umukoro (2014) (IU14 hereafter).

2.1 Remote sensing identification of gas flares

VIIRS is a scanning radiometer for visible and infrared light on board the sun-synchronous Suomi National Polar-orbiting Partnership (Suomi-NPP) weather satellite (NASA, 2016). It can detect combustion sources at night (e.g., bush fires or gas flares) by spectral band M10. To confirm these sources and to eliminate noise, the day/night band, M7, M8 and M12 are used in addition. By fitting these measured spectra to the Planck's radiation curve, background and source temperatures can be deduced (VIIRS, 2015a).

The data are freely available as daily cloud corrected data from March 2014 to present. The files include, among others, the location of the combustion sources, source temperature T_s, radiant heat H and time of observation. VNF does not distinguish between the different combustion sources (e.g., wild fires or flaring). To extract the flaring information from VNF a postprocessing is necessary. For this study we have decided for a 2-month period of observation. This allows for a compilation of a flaring climatology in terms of the locations and emissions and a robust estimation of uncertainty owing to cloud coverage and parameters that have to be prescribed for IU14. We have selected the months of June and July because the gas-flaring emission dataset will be used within the regional online-coupled chemistry model COSMO-ART (Vogel et al., 2009) during the measurement campaign of the project DACCIWA, which took place in June/July 2016. This campaign includes airborne, ground-based and remote sensing observations of meteorological conditions and air pollution characteristics. COSMO-ART is one of the forecasting models of the DACCIWA campaign and delivers spatiotemporal aerosol/chemistry distributions. The data for June/July 2014 and June/July 2015 are used also to allow for an interannual comparison and to assess the uncertainty owing to changes in flare processes (e.g., built-up or dismantling, increase or decrease in combustion). The dataset includes the countries that can affect SWA with their flaring emissions, in particular Ivory Coast, Ghana, Nigeria, Cameroon, Gabon, Congo, the Democratic Republic of the Congo and Angola. The extraction of the flaring information from the VNF data (VNF_{flare} hereafter) was realized by the Earth Observation Group of NOAA. Within VNF_{flare} a file in CSV format file for every SWA flare is available, containing the flaring history in June/July 2014 and 2015. For this study we use the location, source temperature and radiant heat.

2.2 Emission estimation method

The principle emission estimation methodology used in this study follows IU14. The gas-flaring emissions are estimated based on combustion equations for incomplete combustion including six flaring conditions given in Table 1. The equations are introduced in detail in IU14 and are therefore not presented here. This section concentrates on the application of the method of IU14 to the VNF_{flare} data and the research domain SWA.

As input, IU14 needs the natural gas composition C of the fuel input of the flare, the source temperature T_s (temperature in the combustion zone) and the flare characteristics including combustion efficiency η (1 is complete combustion without Carbon monoxide formation) and availability of combustion air δ (above 1 means excess and below 1 means deficiency). In addition we need the flow rate F, the gauge pressure of the fuel gas in the flare p_g and the fraction of total reaction energy that is radiated f. The value for f is estimated by averaging a table of literature values for f given in Guigard et al. (2000). The IU14 input is summarized in Table 2.

The natural gas composition is taken from Sonibare and Akeredolu (2004). They have measured the molar composition of Nigerian natural gas in the Niger Delta area for 10 gas flow stations. For this study we have calculated the average over these stations and merged the data according their number of carbon atoms (Table 3). H_2S fraction is rather low because it was detected only in 2 out of the 10 flow stations.

The source temperature T_s is taken from VNF_{flare}. The combustion efficiency η and the availability of combustion air δ significantly depend on the flaring characteristics (e.g., available technique to steer the flaring process and how the staff takes care of the flaring procedure), which can vary significantly from one side to another. For SWA no information about these parameters is available. The parameter range at least was isolated according to literature values for gas flaring in general (not specifically for SWA). IU14 remarked, that the reaction condition for flaring of $\eta \gg 0.5$ and $\delta \geq 0.9$ should be the norm in regions, where the effective utilization of this gas is not available or not economical. Strosher (2000) indicated a combustion efficiency of solution gas at oil-field battery sites between 0.62, 0.82, and 0.96 for flaring of natural gas in the open atmosphere under turbulent conditions. EPA (1985) shows combustion efficiencies between 0.982 and 1 for measurements on a flare-screening facility. Based on this information the combustion efficiency η was set to 0.8. Regarding the availability of combustion air, we on the one hand follow IU14 with $\delta \geq 0.9$ and on the other hand assume that the flaring conditions are not perfect in SWA, which means that there is a deficiency in combustion air $\delta < 1.0$. Therefore, $\delta = 0.9$ was used for this study. Section 3.3.2 will shed light on the uncertainty that arises from η and δ via a parameter sensitivity study. The authors strongly recommend a careful selection of η and δ since unrealistic combinations (e.g., higher combustion efficiencies with rather low availability of combustion air) can lead to negative NO and NO_2 emissions.

The flow rate, gauge pressure and fraction of radiated heat are not included in the parameterization of IU14 but are necessary to derive the mass emission rates, which can be used as emission data for an atmospheric dispersion model.

The flow rate F ($m^3\,s^{-1}$) is derived from Eq. (1) (VDI 3782, 1985):

$$F = M/(c_p\,(T_S - T_A)), \tag{1}$$

where M is the heat flow in MW, c_p the mean-specific heat capacity of the emissions, T_S the source temperature and T_A the ambient temperature. VDI 3782 (1985) provides a value of the mean-specific heat capacity of

$$c_p = 1.36 \times 10^{-3}\,\mathrm{MW\,s\,m^{-3}\,K^{-1}}, \tag{2}$$

which is derived for a pit coal firing, but VDI 3782 (1985) denotes that this can be used for other flue gases as well since potential deviations are negligible. The value is consistent with the derived mean-specific heat capacity for TP15 with an uncertainty below 5 %. For the ambient temperature T_A we use 298.15 K as a fixed value, representative of the tropical region. Within a sensitivity study regarding the influence of T_A on the heat flow, we have used the averaged heat flow and source temperature of all flares within the time period June/July 2015 and varied the ambient temperature between 293 and 303 K, as a reasonable temperature range in the tropical regions. The resulting maximum difference in the heat flow is $0.0036\,m^3\,s^{-1}$. Therefore, we assume that the uncertainties using a fixed climatological value for the ambient temperature are negligible. For the application of this inventory to other regions the ambient temperature might be adapted. By using Eqs. (1) and (2) the heat flow F can be derived as

$$F = M/\left(1.36 \times 10^{-3}\ (T_S - 298.15)\right), \tag{3}$$

with T_S in K.

We assume that the emitted heat flow M is equal to the total reaction energy of the flare. VNF_{flare} only detects the energy fraction that is radiated H and not the total energy M. By using the radiant heat H (observed by VNF_{flare}) and the factor f (fraction of H to the total reaction energy; Guigard et al., 2000), we estimate M as $H \cdot 1/f$. For the source temperature T_S we use the VNF_{flare} observations.

The estimation of the fuel gas density, which is necessary to transform the flow rate F into an emission, is problematic due to the lack of data concerning the technical setup of the SWA flares. We assume that the dominating flare type is a low-pressure single-point flare. Bader et al. (2011) pointed out that these flares are the most common flare type for onshore facilities that operate at low pressure (below 10 psi (69 kPa) above ambient pressure) and API (2007) remarks

Table 1. Reaction types for incomplete combustion of flared gas, depending on availability of sulfur in the flared gas and the temperature in the combustion zone that determines the formation of NO and NO_2.

Reaction type	Sulfur in flared gas	Source temperature (K)	NO_x formation
1	No	< 1200	no
2	Yes	< 1200	no
3	No	$1200 \leq T_s \leq 1600$	only NO
4	Yes	$1200 \leq T_s \leq 1600$	only NO
5	No	> 1600	NO and NO_2
6	Yes	> 1600	NO and NO_2

Table 2. Variables and parameters needed for IU14 or for deriving the fluxes of the air pollutants.

Parameter	Description	Reference	Unit
C	Natural gas composition	Sonibare and Akeredolu (2004)	%
T_s	Source temperature	VNF_{flare} (VIIRS, 2015a)	K
η	Combustion efficiency	0.8 (IU14)	–
δ	Availability of combustion air	0.95 (IU14)	–
H	Radiant heat	VNF_{flare} (VIIRS, 2015a)	MW
F	Flow rate	VNF_{flare} (VIIRS, 2015a), (VDI 3782, 1985)	$m^3\ s^{-1}$
p_g	Gauge pressure	34.475 (API, 2007)	kPa
f	Fraction of radiated heat	0.27 (Guigard et al., 2000)	–

Table 3. Molar composition of natural gas in Niger Delta (Nigeria) based on the measurements of Sonibare and Akeredolu (2004), averaged over 10 flow station. The hydrocarbons are merged according to the number of C atoms.

Constituent	Fraction (%)
Methane (CH_4)	78.47
Ethane (C_2H_6)	6.16
Propane (C_3H_8)	5.50
Butane (C_4H_{10})	5.19
Pentane (C_5H_{12})	3.95
Hexane (C_6H_{14})	0.36
Carbon dioxide (CO_2)	0.305
Nitrogen (N_2)	0.06
Hydrogen sulfide (H_2S)	0.005

that most subsonic-flare seal drums operate in the range from 0 to 5 psi (34 kPa). Therefore, we have decided for a gauge pressure p_g of 5 psi (34 kPa) above ambient pressure. Via Eq. (4) we can calculate the fuel gas density ρ_f

$$\rho_f = p_f / (R / (M_f T_A)), \quad (4)$$

where p_f is the fuel gas pressure as the sum of ambient pressure (10.1325 kPa, taken as const) and gauge pressure p_g. R is the universal gas constant, M_f the molar mass of the fuel gas and T_A the ambient temperature (298.15 K, taken as const). Finally, the emission E ($kg\ s^{-1}$) of a species i is given by

$$E_i = \frac{m_i}{m_{total}} \rho_f F, \quad (5)$$

where m_i is the mass of the species i and m_{total} the total mass of the fuel gas, both delivered by the parameterization of IU14.

The combustion calculations within IU14 provide the species water, hydrogen, oxygen, nitrogen, carbon monoxide, carbon dioxide, sulfur dioxide, nitrogen oxide and nitrogen dioxide. In the following only the latter five are considered. However, no black carbon or volatile organic compounds (VOCs) are considered by IU14, although they are not negligible. Johnson et al. (2011) estimated the mean black carbon emission for a large-scale flare at a gas plant in Uzbekistan to be $7400\ g\ h^{-1}$, and Strosher (1996) measured the concentration of predominant VOCs 5 m above the gas flare in Alberta with $458.6\ mg\ m^{-3}$. However, owing to the missing representation of black carbon and VOCs in IU14, these compounds are not considered in this study.

By using the source code written in R (R Core Team, 2013) delivered by this study, the user can define the grid size independently (e.g., model grid) on which the flaring point sources are allocated.

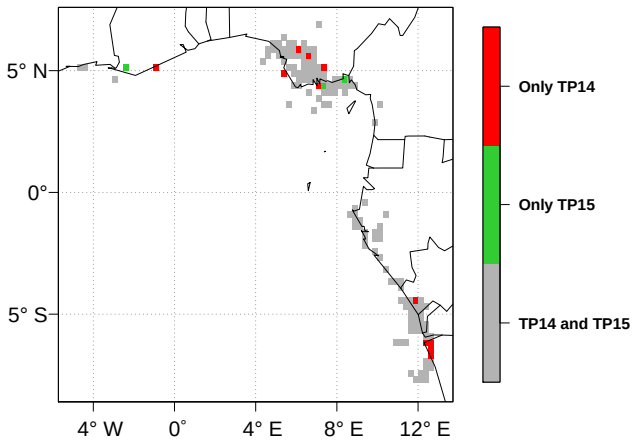

Figure 1. Flaring area for TP14 and TP15. Red (green) boxes denote areas with flaring only for TP14 (TP15). For the gray areas, flaring is detected in both time periods.

3 Results

3.1 Spatial distribution of gas flaring in SWA

We have selected the two time periods, June/July 2014 (TP14) and June/July 2015 (TP15), of VNF_{flare} over SWA (61 observations).

In the preparation of this work, we have compared the locations of the flares of TP14 with the Google Earth imagery (Google Earth, 2014) (not shown). Only the onshore flares are visible in Google Earth. This visual verification reveals that 72 % of the VNF_{flare} detected onshore flares are visible in Google Earth. It is very likely that the hit rate is much higher since it is often the case that the Google Earth image quality is not good enough for verification or the images are not up to date. This comparison indicates that VNF_{flare} is an effective method to identify the flares in SWA.

For the following analysis we have allocated the flares to a grid with a mesh size of 0.25° (28 km) from 8° S to 7° N and from 5° W to 13° E and calculated the emissions for both time periods. A grid box with flaring is denoted as flare box hereafter. Figure 1 emphasizes the areas in which VNF_{flare} detects flares only in TP14 (TP15) in red (green) and in gray the areas with flaring in both periods.

Remarkable are the dominating flaring areas in the Niger Delta and the adjacent offshore regions in the Gulf of Guinea. Also in the coastal region of Gabon, Congo and Angola, as well as sporadically in Ghana and offshore of Ivory Coast, flaring occurs. By comparing TP14 and TP15 more red than green areas are visible, especially in southern Nigeria, which indicates a reduction in the flaring area from 2014 to 2015. The red areas contribute 12 % to the total CO_2 emissions of TP14. VNF_{flare} detects 335 flares in 2014 and 312 flares in 2015, which means a reduction of about 7 % (counted are those which deliver at least once a value for T_s and H in the time period). In total, 61 % of that reduction is related to Nigeria. A decrease in CO_2 from 1994 to 2010, particularly in the onshore platforms, is indicated by Doumbia et al. (2014).

Figure 2 shows the density of flares (a) and the flaring activity (b) per flare box for TP15. The results are similar to TP14; therefore, only the TP15 is displayed here.

The highest flare density can be found offshore in the border area of Nigeria and Cameroon with 17 flares per flare box. The offshore flaring density is smaller than onshore (Fig. 2a), whereas the highest flaring activity can be found offshore (Fig. 2b). This could be linked to the increased masking of flares by clouds over land. The large onshore flaring area of the Niger Delta shows a comparable low-flaring activity of 10–30 %. The highest values can be found offshore of the Democratic Republic of the Congo and Angola at 50–90 %. How the interannual variability of flaring reflects in the amount of flaring emissions is analyzed in Sect. 3.3.4.

3.2 Emission estimation

For the emission estimation we have used a climatological approach (E_{clim}). For every flare the temporal averages of source temperature and radiant heat over TP14 and TP15 were used to calculate the emissions. Therefore, in this approach all flares, detected in the time period, are active at once with their mean emission strength. This method has the advantage that most likely all flares in the domain are captured even if a fraction of them is covered by clouds at certain days. However, this could lead to an emission overestimation because not all available flares are active at once. This problem of separating between flares that are not active and flares that are active but covered by clouds and therefore not visible for VNF_{flare} is picked up again in Sect. 3.3.1. Figure 3 shows the emissions of CO_2, CO, SO_2, NO and NO_2 in $t\,h^{-1}$ for TP15.

The highest emissions are derived for carbon dioxide, followed by carbon monoxide, nitrogen dioxide and nitrogen oxide. Sulfur dioxide shows the lowest emissions since these emissions do not depend on combustion processes but only on the natural gas composition (see Table 3) and the amount of flared gas (IU14). Due to the use of the averaged measurements of Sonibare and Akeredolu (2004), local variations of hydrogen sulfide concentrations in the natural gas cannot be taken into account. Hydrogen sulfide is the only source of sulfur in the flared gas and therefore determines the emission of sulfur dioxide. To assess this uncertainty, a sensitivity study with different hydrogen sulfide concentrations is given in Sect. 3.3.5.

3.3 Estimation of uncertainties

In the following section the most relevant uncertainties are presented together with approaches for their assessment. This includes the uncertainty concerning the flare detection

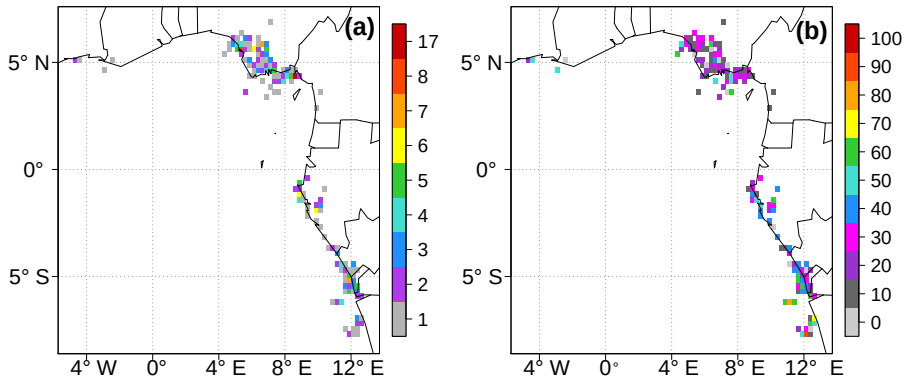

Figure 2. **(a)** Number of flares per flare box and **(b)** flaring activity (%) per flare box within TP15. A flaring activity of 100 % means that every day in the 61-day period in June/July flaring was detected.

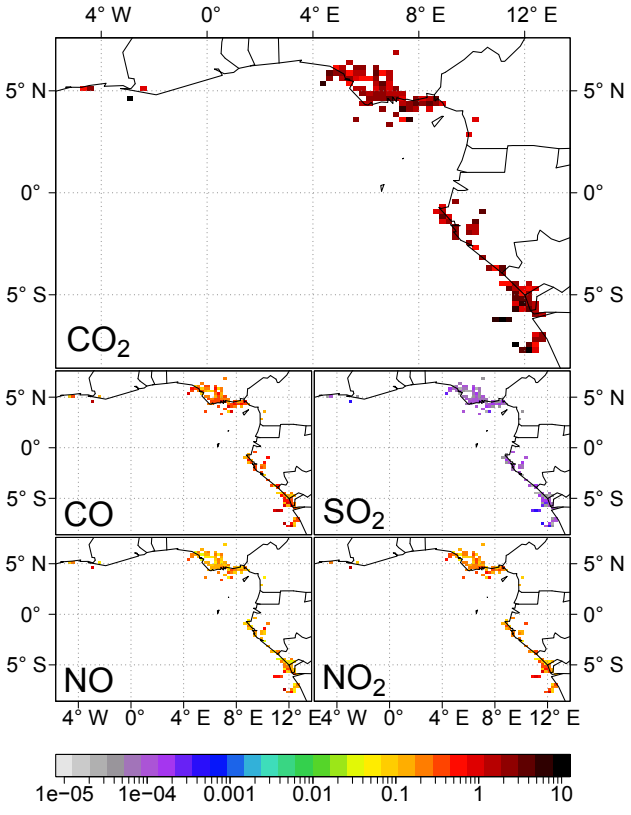

Figure 3. Flaring emissions for TP15 within E_{clim} in $t\,h^{-1}$ considering CO_2, CO, SO_2, NO and NO_2. For better visibility the emissions are displayed as colored grid boxes although the emissions are still point sources and not area sources.

in the presence of cloud cover, the uncertainty in the determination of the emitted heat flow H via the fraction of radiated heat f, the uncertainty in the choice of the IU14 parameters and the changes in flare operation from one year to another as well as the influence of the spatial variability of hydrogen sulfide in the natural gas on the sulfur dioxide emissions.

Apart from Sect. 3.3.4 all uncertainty estimations are confined to TP15.

3.3.1 Uncertainty due to cloud cover

In this section we want to estimate the emission error due to cloud-covered flares and present a method to derive daily emissions by considering the contribution of these masked flares. In Sect. 3.2, a climatological dataset of flaring emissions (E_{clim}) was derived, in which all available flares are active with their mean emission strength. This dataset therefore does not include a day-to-day variation. If an emission dataset with a daily variability is required, the problem arises that usually parts of the scene observed by the satellite are covered by clouds and therefore the emissions are likely underestimated. VNF_{flare} includes the locations of all flares independent of whether they are active or not. This entity is illustrated by the closed dark gray pie in Fig. 4a and b. By comparing the flares that are observed/active at a certain day and the total number of flares, a separation between observed (green pie in Fig. 4a) and not observed (light gray pie in Fig. 4a) is possible. In addition VNF_{flare} delivers a cloud mask for all of the flare detections. Therefore, it is possible to separate the light gray pie of the not observed flares in (a) cloud-free and inactive (light blue pie in Fig. 4b) and (b) cloud-covered and unknown flaring status (blue pie in Fig. 4b).

To estimate the error due to active but cloud-covered flares, we assume that all of these flares are active with their mean emission strength observed in June/July 2015.

Figure 5 illustrates the mean cloud cover exemplarily for the greater Niger Delta area using (a) instantaneous cloud fractional cover from the geostationary Meteosat Second Generation 3 (MSG3) (CM SAF, 2015, copyright (2015) EUMETSAT) for every day of TP15 around the time of VNF observation (Suomi-NPP overflight approx. at 01:00 UTC) and (b) the sun-synchronous Aqua/AIRS (Mirador, 2016).

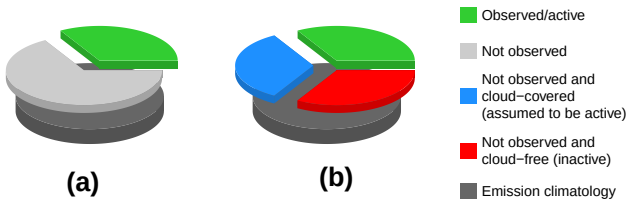

Figure 4. Pie charts illustrating the flaring emission uncertainty assessment due to cloud cover for TP15. The entity of the flares within the emission climatology (E_{clim}) is given as a closed gray pie in the bottom of **(a)** and **(b)**. Panel **(a)** distinguishes between flares which are detected/active at a certain day (green) and the complement of undetected flares (light gray). In **(b)** the light gray slice of **(a)** is separated in a cloud-covered (blue) and cloud-free (red) part by using the cloud mask of VNF_{flare}. Flares that are not detected by VNF_{flare} and covered by clouds are taken as active. Flares that are not detected by VNF_{flare} and are not covered by clouds are taken as inactive.

Figure 5a shows that the onshore flaring area for TP15 is in mean covered with clouds by 50–70 %. For the offshore flaring area it is even higher with 70–90 %. Therefore ,it is very likely that flares are frequently masked by clouds and therefore not detected by VNF. However, we suspect that the MSG3 cloud product underestimates (overestimates) the onshore (offshore) cloud cover when compared with the findings of van der Linden et al. (2015). The high offshore coverage and the distinct land–water separation might be caused by overestimating low clouds in the presence of a warm and moist tropical ocean.

Figure 5b shows a cloud climatology using Aqua/AIRS nighttime data (Mirador, 2016). The Aqua/AIRS climatology shows higher cloud cover over land and no distinct separation between water and land surface. Both products identify the highest onshore cloud cover in the northeast of Port Harcourt (4.8° N, 7.0° E) and have similar values in the Nigerian offshore region (containing the offshore flares) of about 70–80 %. The major difference in the climatologies appears onshore between 4.5 and 6° N. This area includes the majority of the Nigerian onshore flares. This reveals a relatively high uncertainty in the estimation of nocturnal low cloud coverage from remote sensing.

Figure 6 shows the number of flares per day in TP15, separated in the categories: cloud-free/active (green), cloud-free/inactive (red) and cloud-covered (blue). Flares with no or incomplete data are coded in black. E_{clim} includes 312 flares, which are at least once active in TP15. On average only 26 % of the total flaring area is active at once, 9 % is verifiable inactive and 63 % is cloud-covered. By taking into account only the cloud-free information instead of the climatological approach of E_{clim}, on average 63 % of the flares are not considered at a certain day. By assuming that all of these cloud-covered flares are active, a remarkable underestimation can be expected.

In addition to E_{clim} two further emission inventories are introduced; E_{obs} only considers the actual daily observed flares (linked to the green flares in Fig. 6). To consider also the contribution of active but cloud-covered flares, E_{com} combines the green and the blue flares of Fig. 6.

To allow for consistency, all three inventories use the emissions derived from the flare-specific temporal averages of the source temperature and the radiant heat over TP14 and TP15, respectively.

We avoid calculating the emissions from instantaneous source temperatures because this is linked to high uncertainty depending on the atmospheric conditions (M. Zhizhin, personal communication, 2016). The temporal averages allow for robustness. Therefore, the three inventories only differ in the selection of the active flares per day but not in the underlying emissions. E_{clim} uses all flares at a certain day, E_{obs} considers only the flares that are cloud-free and active and E_{com} considers E_{obs} plus the cloud-covered flares, by assuming that all of the cloud-covered flares are active. Nevertheless, we have included a further inventory in Table 5, which uses instantaneous source temperature and radiant for the emission derivation (E_{clim}, instantaneous input) to assess the differences towards the averaged input. Figure 7 shows the total CO_2 emissions of the SWA area from E_{clim} in black, from E_{obs} in green and from E_{com} in blue.

The dashed lines denote the temporal averages of E_{obs} and E_{com}. On average E_{com} is only 9 % smaller than E_{clim}, which is assumed to be in the range of uncertainty. Therefore, both inventories are equitable in this study. The user can decide whether a temporal resolved or a climatological approach fits best to their research question.

The emissions of E_{obs} are strongly reduced (64 %) compared to E_{clim} as expected. The use of E_{obs} would significantly underestimate the emissions and is therefore not appropriate for an application. Since E_{obs} does not take into account cloud-covered flares at all and E_{com} in contrast sees all cloud-covered flares as active, the difference between these inventories can be used to assess the uncertainty arising from flares masked by clouds. Figure 7 shows a mean difference between E_{obs} and E_{com} of about 61 %. Therefore, while using E_{obs} as a flaring emission inventory in an application, an underestimation of the emissions of 61 % has to be considered.

These emission estimations contain different information. E_{clim} includes all flares of the domain invariant but can overestimate the emissions. E_{obs} shows the VNF_{flare} reality, including a temporal development, but cannot consider the cloud-covered flares. E_{com} combines the climatological information of E_{clim} for flares that are not observable at a certain time and the temporal resolution of VNF_{flare} in E_{obs}. However, this approach is based on the assumption that all cloud-covered flares are active, which can be seen as an estimation upwards. Therefore, the most likely amount of emissions is expected between E_{obs} and E_{com}.

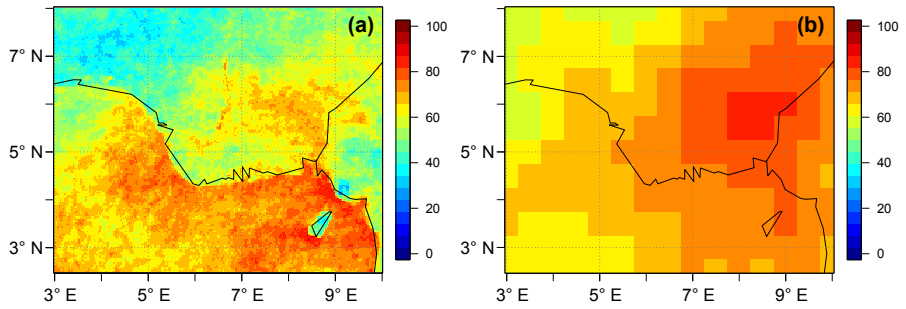

Figure 5. Fractional cloud cover (%) observed from **(a)** the geostationary MSG3 and **(b)** the sun-synchronous Aqua/AIRS, averaged over TP15 around the time of VNF observation (approx. 01:00 UTC).

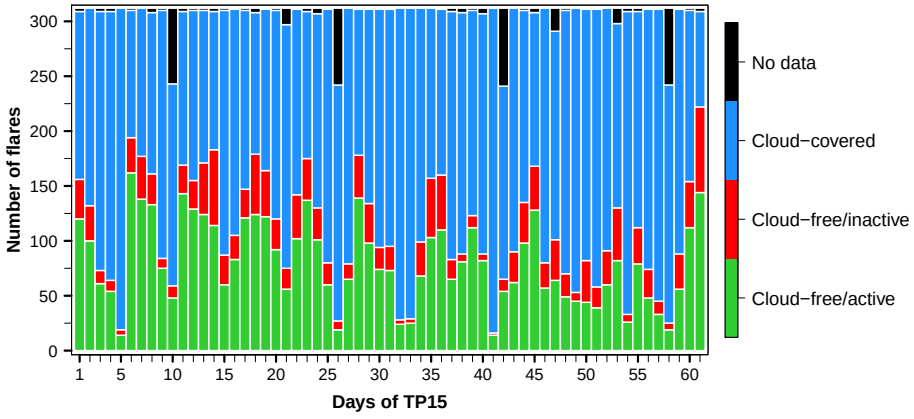

Figure 6. Number of flares per day in TP15 that are cloud-free and active (green), cloud-free and inactive (red) and cloud-covered (blue). Flares with no or incomplete data are denoted in black. The color coding follows Fig. 4b. Considered are the 312 flares that deliver at least once a value for T_s and H in TP15.

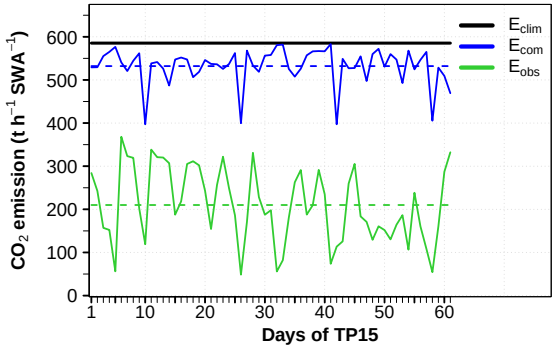

Figure 7. Daily CO_2 emission estimations ($t\,h^{-1}$) within TP15 from flaring, summed up over the SWA area as denoted in Fig. 1 for the three emission inventories: E_{clim} (climatology, black solid line), E_{obs} (daily VNF_{flare} observations, green solid line and temporal average as green dashed line) and E_{com} (sum of daily VNF_{flare} observations and emissions from cloud-covered flares, blue solid line and temporal average as blue dashed line). The periodical drop of the blue line is linked to reduced data coverage (compare with black bars in Fig. 6).

3.3.2 Uncertainty due to IU14 input parameters

To assess the uncertainty that arises from the combustion efficiency η and the availability of combustion air δ, a sensitivity study has been carried out. The exact values for the SWA flares are unknown and very likely highly variable from one flare to another, depending on the flare type and operation. Figure 8a shows the flaring emissions averaged over SWA and TP15 for CO, CO_2, NO and NO_2. The parameters η and δ are varied referring to IU14. A complete combustion ($\eta = 1$) does not produce CO emissions since all carbon is transformed to CO_2 (not shown). With decreasing η and δ, the CO and CO_2 emissions increase. Concerning CO, we assume the lower limit for $\eta = 0.9$ and $\delta = 1.3$ (left of Fig. 8a) and the upper limit for $\eta = 0.5$ and $\delta = 0.76$ (right of Fig. 8a). The values used for this study are located in the center of Fig. 8a (printed in bold). By taking the latter as reference, the lower (upper) limit leads to a decrease (increase) in CO emission of $-63\,\%$ ($+208\,\%$). For CO_2 we derived a lower (upper) limit of $-53\,\%$ ($+12\,\%$).

A higher availability of combustion air allows for an enhanced formation of NO and NO_2. Therefore, NO_x emis-

sions increase with decreasing η. In contrast these emissions decrease with an increase in the combustion efficiency (δ). The higher the efficiency the more oxygen is forming CO_2 instead of NO_x. We assume the lower limit for $\eta = 0.9$ and $\delta = 0.95$ and the upper limit for $\eta = 0.5$ and $\delta = 1.30$. Taking again the central parameter set of Fig. 8a as reference, the lower (upper) limit leads to a decrease (increase) in NO emission of $-76\,\%$ ($+420\,\%$).

For NO_2 the emission decrease (increase) is $-76\,\%$ ($+417\,\%$).

In addition, Fig. 8b shows the emissions depending on the gauge pressure for 1 (lower limit), 5 and 10 psi (upper limit) (7, 34 and 69 kPa, respectively) for $\eta = 0.8$ and $\delta = 0.95$. Using 5 psi as the reference, the lower (upper) limit leads to a decrease (increase) in CO emissions of $-20\,\%$ ($+25\,\%$).

Figure 8 emphasizes that the technical conditions of flaring crucially influence the emission strength and that the emissions are more sensitive towards η and δ than towards the gauge pressure.

3.3.3 Uncertainty due to the fraction of radiated heat

To estimate the uncertainty in the fraction of radiated heat f (see Table 2), we have used the standard deviation of the literature values given in the appendix of Guigard et al. (2000) in addition to the mean value of $f = 0.27$. This leads to a domain of uncertainty for the value f of (0.38/0.16). Therefore, the VNF_{flare} observed radiant heat is multiplied with the factor $1/f$ of 3.7 (6.2/2.6).

3.3.4 Interannual variability

The differences in flaring between TP14 and TP15, indicated in Figs. 1 and 2, are quantified in this section according to the emissions of CO (Fig. 9a) and CO_2 (Fig. 9b). The box plots include all flares for the two domains SWA (green) and Nigeria (blue). The numbers above indicate the integrated emissions per hour and area in tons.

The emissions of CO_2 are 6.3 times higher than the CO emissions. For Nigeria (blue box plots) the mean value of emissions is statistically significantly lower for TP15 compared to TP14 (Wilcoxon–Mann–Whitney rank sum test with a significance level of 0.05). For SWA the emission averages show no significant difference. The significantly different mean values for Nigeria emphasize the relevance of using a flaring dataset, which is up to date to reduce uncertainties arising from deviations in flare locations or flaring processes.

3.3.5 Uncertainty due to spatial variability in H_2S

Since hydrogen sulfide (H_2S) is the only sulfur source in the flared gas, it determines the emission of sulfur dioxide. The natural gas composition measurements from the 10 flow stations given in Sonibare and Akeredolu (2004) contain only two stations with nonzero H_2S content. Therefore, averaging over the 10 stations (see Table 3) leads to a low-H_2S content in the emission calculations. By using the highest concentration value of H_2S given in Sonibare and Akeredolu (2004) (see Table 3; H_2S concentration 0.03 % instead of 0.005 %), we try to estimate the upper limit of SO_2 emission, assuming that all flares are provided with this more sulfur containing gas. With this approach the temporal-averaged sum of SO_2 emissions over SWA increase from 36 to $320\,kg\,h^{-1}$. This comparison reveals that among the flaring conditions also the natural gas composition plays an important role in estimating the flaring emissions reasonably. To rely on a single-measurement dataset for a large flaring domain and without taking into account spatial variability is therefore problematic but has to be accepted owing to data shortage.

This section has estimated the uncertainties in gas flaring due to cloud cover, parameters of IU14, the fraction of radiated heat, the temporal variability and the H_2S concentration in the natural gas. The uncertainty regarding the spatial variability of the total hydrocarbon fraction of the natural gas, which is estimated by the variations in the 10 flow station measurements of Sonibare and Akeredolu (2004), is below 1 %.

However, there are further assumptions or sources of uncertainty that cannot be quantified within this study; we assume that the natural gas composition, which is measured in one region, is valid for SWA entirely. The gas flares are taken as constant emission sources because VNF_{flare} only provides one observation (overflight) per day. We cannot take into account the spatial variability of the flares concerning the IU14 parameters and the stack heights. Finally, IU14 delivers no VOCs and black carbon.

4 Comparison with existing emission inventories

The following section places the estimated flaring emissions of this study in the context of existing emission inventories by focusing on CO_2. A direct comparison with existing emission inventories is problematic due to different reference time periods, spatial domains, definitions of emission sectors and the limitation of chemical compounds. Table 4 summarizes the CO_2 emissions for different inventories regarding Nigeria as the flaring hotspot of the research domain. To derive annual emission values for the results of this study, it is assumed that the flaring emission conditions of TP14 and TP15 are representative for the whole year 2014 and 2015, respectively. Therefore, the hourly emissions are integrated over 365 days. In addition to the three inventories E_{obs}, E_{com} and E_{clim}, whose emissions are derived from temporal averages of the source temperature and radiant heat, also an emission estimation using instantaneous source temperature and radiant heat (calculating emissions for every single observation and subsequent temporal averaging of the emissions) for both time periods is presented in Table 4 (E_{clim}, instantaneous input).

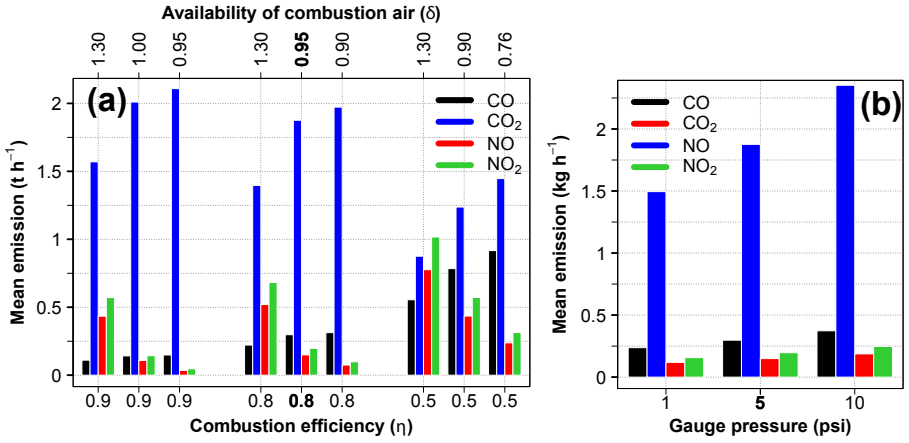

Figure 8. Flaring emissions ($t\,h^{-1}$) spatiotemporally averaged over SWA and TP15 depending on **(a)** combustion efficiency η and availability of combustion air δ for a gauge pressure of 5 psi and **(b)** gauge pressure (psi) for $\eta = 0.8$ and $\delta = 0.95$. SO_2 is not shown because it does not depend on η or δ.

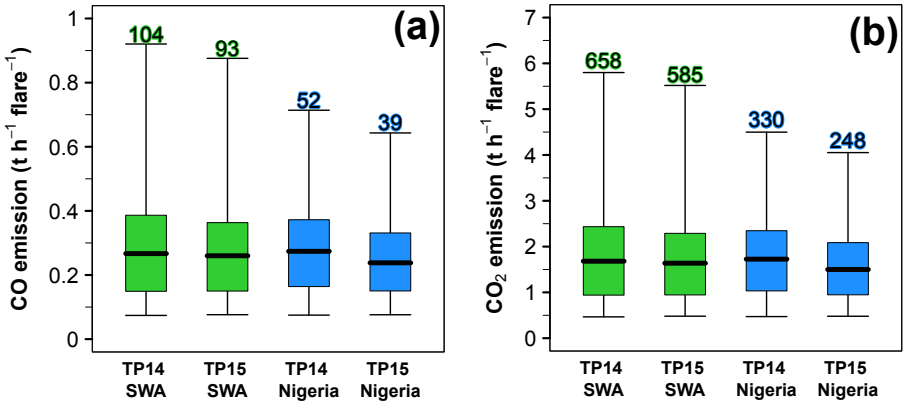

Figure 9. Single flaring emissions of **(a)** CO and **(b)** CO_2 (E_{clim}, $t\,h^{-1}$ $flare^{-1}$) for SWA (green) and Nigeria (blue) for TP14 and TP15. The values above the box plots indicate the emissions per hour, integrated over SWA (green) and Nigeria (blue). The whiskers span the data range from the 0.025 quantile to the 0.975 quantile (95 % of the data). Data outside of this range is not shown.

The CO_2 emission estimations of this study are given in Table 4 together with an overall uncertainty range of (+33/−79 %) in parentheses, including the uncertainty from the IU14 parameters η and δ (+12/−53 %) and the gauge pressure (+20/−25 %) and from spatial variability of total hydrocarbon. The latter uncertainty is small (below 1 %) owing to the low variation in total hydrocarbon (THC) concentration in the measurements of Sonibare and Akeredolu (2004). The uncertainty owing to the fraction of radiated heat f is represented by using the average value of 0.27 and the upper and lower estimate of 0.16 and 0.38, respectively. The uncertainty due to cloud cover is represented by the difference in E_{obs} and E_{com}.

By assuming that E_{com} with $f = 0.27$ represents the best emission estimate for this study and by integrating the abovementioned sources of uncertainty, a total Nigerian CO_2 flaring emission of 2.7 (3.6/0.5) Tg yr^{-1} for 2014 and 2.0 (2.7/0.4) Tg yr^{-1} for 2015 was derived. Due to the high uncertainties, the two estimates are not statistically different. These values are 1 order of magnitude smaller than the values from the Carbon Dioxide Information Analysis Center (CDIAC, 2015b), the Energy Information Administration (EIA, 2015) and the EDGARv.4.3.2 (EDGAR, 2016) database. A direct comparison is hindered by a time lag of 3–4 years and missing information about the uncertainties of CDIAC. The values of EIA are higher than those of CDIAC because EIA includes the consumption of natural gas in addition to gas flaring. Doumbia et al. (2014) combined DMSP observations of flaring with the emission factor method to derive flaring emissions. The results agree with EIA (2015) but are 64 % higher than CDIAC (2015b).

The emission inventory EDGAR v4.2 (ECCAD, 2015) delivers 8.75 (3.50) Tg CO_2 yr^{-1} for Nigeria (Niger Delta area)

Table 4. Comparison between existing emission inventories for CO_2 (with a focus on gas flaring if available) and the results of this study for Nigeria in teragrams (Tg) per year. For TP14 and TP15 it is assumed that the 2-month observations represent the flaring conditions of the whole year 2014 and 2015, respectively. Therefore, the emissions were integrated to yearly values. The domain of uncertainty arising from the UP14 parameters and the spatial variability in total hydrocarbon is given in parentheses. For the fraction of radiated heat f, the mean value 0.27 and the lower (upper) boundary of 0.16 (0.38) are used, representing a further source of uncertainty. The products given in bold are directly related to flaring emissions.

Emission inventory	Time period	CO_2 emissions ($Tg\,yr^{-1}$)		
		$f = 016$	$f = 027$	$f = 038$
This study (E_{obs}, averaged)	2014 (from TP14)	1.7 (2.2/0.3)	1.0 (1.3/0.2)	0.7 (1.0/0.1)
This study (E_{com}, averaged)	2014 (from TP14)	4.5 (6.1/0.9)	2.7 (3.6/0.5)	1.9 (2.6/0.3)
This study (E_{clim})	2014 (from TP14)	4.9 (6.5/1.0)	2.9 (3.9/0.6)	2.1 (2.8/0.4)
This study (E_{obs}, averaged)	2015 (from TP15)	1.0 (1.4/0.2)	0.6 (0.8/0.1)	0.4 (0.6/0.0)
This study (E_{com}, averaged)	2015 (from TP15)	3.4 (4.5/0.7)	2.0 (2.7/0.4)	1.4 (2.0/0.3)
This study (E_{clim})	2015 (from TP15)	3.7 (4.9/0.7)	2.2 (2.9/0.4)	1.5 (2.1/0.3)
This study (E_{clim}, instantaneous input)	2014 (from TP14)	9.9 (13.2/2.0)	5.9 (7.9/1.2)	4.2 (5.6/0.8)
This study (E_{clim}, instantaneous input)	2015 (from TP15)	8.8 (11.8/1.8)	5.2 (7.0/1.0)	3.7 (4.9/0.7)
CDIAC (2015b)[1]	2011			27.47
EIA (2015)[2]	2010; 2011; 2013		38.81; 41.39; 52.83	
Doumbia et al. (2014)[1]	2010		45	
EDGAR 4.2[3] (ECCAD, 2015)	2008		8.75	
EDGAR 4.2[4] (ECCAD, 2015)	2008		3.50	
EDGAR 4.3.2[5] (EDGAR, 2016)	2010; 2011; 2012		29.4, 28.8, 28.9	
EDGARv43FT2012[6] (EDGAR, 2014)	2014		93.87	

[1] From gas flaring, Nigeria
[2] From consumption and flaring of natural gas
[3] From refineries and transformation, Nigeria
[4] From refineries and transformation, Niger Delta area according to Fig. 5a
[5] From venting and flaring of oil and gas production, Nigeria
[6] Emission totals of fossil fuel use and industrial processes (cement production, carbonate use of limestone and dolomite, non-energy use of fuels and other combustion). Excluded are short-cycle biomass burning (such as agricultural waste burning) and large-scale biomass burning (such as forest fires), Nigeria

for the emission sector *refineries and transformation*, which is in good agreement with the results for the study on hand.

As a benchmark for the flaring CO_2, the total CO_2 emissions for Nigeria are given by EDGAR (2014) (fossil fuel use and industrial processes). Taking EDGAR (2014) as a reference for total CO_2 emissions of Nigeria, flaring emissions contribute with 2 % (3.9/0.0) % (this study for 2014; E_{com}), 9 % (2008; ECCAD, 2015), 28 % (2011; CDIAC, 2015b), 48 % (2010; Doumbia et al., 2014) or 56 % (2013; EIA, 2015). The large spread between the different inventories emphasizes the large uncertainty within the estimation of emissions from gas flaring.

By using the climatological approach with instantaneous source temperature and radiant heat input data (E_{clim}, instantaneous input) instead of temporal averages (E_{clim}), the emissions are increased by approximately a factor of 2 (5.9 (7.9/1.2) $Tg\,yr^{-1}$ for 2014, 5.2 (7.0/1.0) $Tg\,yr^{-1}$ for 2015). This underlines that also the preprocessing of the remote sensing data for the calculation of the emissions is a considerable source of uncertainty. However, due to the high uncertainties also the two emission estimates with and without instantaneous data are not statistically different.

A shortcoming of the PEGASOS_PBL-v2 (not shown) and the EDGAR v4.2 emission inventory is the lack of offshore flaring emissions in the Gulf of Guinea south of Nigeria. For CDIAC and EIA this cannot be verified since the data are only available as a single value per country.

The differences between the results of this study and the existing emission inventories might be caused by insufficient information about the efficiency of combustion processes of SWA flares or by an inconsistent definition of emission source sectors for the existing inventories. E_{com}, Doumbia et al. (2014) and CDIAC (2015b) focus on gas flaring, whereas other products also include natural gas consumption and emissions from refineries and transformation, which also can include non-flaring emissions within and outside the areas indicated as flaring area by the satellite imagery. In addition, the existing inventories do not provide current values (time lag of 2 to 6 years) and therefore do not consider the emission reduction indicated by Fig. 9.

5 Discussion and conclusions

The gas-flaring emission estimating method of Ismail and Umukoro (2014) (IU14) has been combined with the remote

sensing flare location determination of the VIIRS Nightfire (VNF) prerun V2.1 flares only (VIIRS, 2015a) for a new flaring emission parameterization. The parameterization combines equations of incomplete combustion with the gas flow rate derived from remote sensing parameters instead of using emission factors and delivers emissions of the chemical compounds CO, CO_2, SO_2, NO and NO_2.

Within this study the parameterization was applied to southern West Africa (SWA) including Nigeria as the second biggest flaring country. Two 2-month flaring observation datasets for June/July 2014 (TP14) and June/July 2015 (TP15) were used to create a flaring climatology for both time periods. In this climatology all detected flares emit with their mean activity (climatological approach).

The uncertainties owing to missed flare observations by cloud cover, parameterization parameters, interannual variability and the natural gas compositions were assessed. It can be shown that the highest uncertainties arise from the IU14 parameters ($+33/-79\,\%$), followed by the definition of the fraction of radiated heat f. The uncertainty arising from flares masked by clouds is estimated as 61 % on average in TP15.

By using the cloud detection of VNF and by assuming that all cloud-covered flares are active, an additional emission dataset was derived that combines the emissions from the currently observed flares and the climatological emissions from cloud-covered (not detected) flares (combined approach). These emissions are on average 9 % smaller than the climatology but 61 % larger than the net observations.

However, owing to the large uncertainty ranges, no significant difference between the climatological inventory and the combined inventory can be stated. Comparing the emissions of 2014 and 2015, a reduction in the flaring area, density of active flares and a significant reduction in Nigerian flaring emissions of about 25 % can be observed, which underlines the need for more recent emission inventories.

The uncertainty due to the natural gas composition is compound dependent. The spatial variation in total hydrocarbon is negligible but the availability of hydrogen sulfide, which exclusively determines the amount of emitted SO_2, cause large uncertainty. By taking the combustion efficiency to derive the fraction of unburned natural gas, the amount of emitted VOCs might be estimated in addition to the species of the study on hand but would also be linked to high uncertainties concerning the VOC speciation. The uncertainty in VOC emission is increased drastically by natural gas, which is vented directly into the atmosphere instead of being flared, since the venting cannot be detected by VNF.

With a focus on Nigeria, the CO_2 emission estimates of this study were compared with existing inventories. For the combined approach, CO_2 emissions of 2.7 (3.6/0.5) Tg yr^{-1} for 2014 and 2.0 (2.7/0.4) Tg yr^{-1} for 2015 were derived. EDGAR v4.2 for the year 2008 shows the same order of magnitude when limited to emissions from refineries and transformation. The results of this study are 1 order of magnitude smaller compared to CDIAC (Carbon Dioxide Information Analysis Center), Doumbia et al. (2014) and EIA (Energy Information Administration). This emission underestimation is not caused by an underestimation of the flared gas volume. VNF_{flare} includes an estimation of the annual sum of flared gas by country. For Nigeria the estimated values are 8.56 (7.64) bcm flared gas in 2014 (2015). Within this study higher values of 37.89 (20.68) bcm for 2014 (2015) are derived.

The deviations might be caused by the uncertainty in the efficiency of the flares concerning the combustion process and their operation. A lack of information regarding the combustion efficiency together with the high sensitivity of the parameters within the combustion equations of IU14 can lead to high uncertainties. Additionally, the usage of emission factors in the existing inventories, which did not take into account the spatiotemporal variability of flaring, inconsistent emission sector definitions or the time lag of the emission inventories of 2–5 years, can cause deviations. The positive trend in Nigerian gas-flaring CO_2 emissions derived by EIA from 38.81 to 52.83 Tg yr^{-1} between 2010 and 2013 contradicts the findings of Doumbia et al. (2014) and this study, which generally show a decrease in emissions from 1994 to 2010 and from 2014 to 2015, respectively. Based on the sensitivity study, which reveals high uncertainties of the flaring emission, we conclude that there is no preference in the choice of the climatological and or the combined approach presented in this study. Therefore, for simplicity we recommend the use of the climatological approach when using the R package.

Despite the generally large uncertainties in the estimation of emissions from gas flaring, this method allows for a flexible creation of flaring emission datasets for various applications (e.g., as emission inventory for atmospheric models). It combines observations with physical-based background concerning the combustion. The use of current data makes it possible to consider present trends in gas flaring. Even the creation of near-real time datasets with a time lag of 1 day is possible. The emissions are merged on a grid predefined by the user and depending on the availability of VNF data, the temporal resolution can be selected from single days to years.

An improvement of this parameterization can be achieved by an extension of the IU14 method to black carbon and VOCs and an inclusion of spatially resolved measurements of the natural gas composition in combination with information of the gas-flaring processes from the oil producing industry. Gas flaring is just one of the sources of air pollution in SWA and therefore the DACCIWA field campaign in June–July flaring cannot solely focus on flaring. To provide detailed measurements of the flaring characteristics would go beyond the scope of DACCIWA. However, within the DACCIWA aircraft campaign, the EUFAR (European Facility for Airborne Research) mission APSOWA (Atmosphere Pollution from Shipping and Oil platforms in West Africa) was

conducted to characterize gaseous and particulate pollutants emitted by shipping and oil and gas extraction platforms off the coast of West Africa. The authors hope that the results of APSOWA bring further insight into the characteristics of gas flaring in SWA.

Code and data availability. This publication includes a package of well documented R scripts which is free available for research purposes and enables the reader to create their own gas-flaring emission datasets. It includes exemplarily the preprocessing for June/July 2015 with a focus on southern West Africa. You get access to the code via https://www.zenodo.org/ (doi:10.5281/zenodo.61151, Deetz and Vogel, 2016), entitled "Gas flaring emission estimation parameterization v2".

Competing interests. The authors declare that they have no conflict of interest.

Acknowledgements. The research leading to these results has received funding from the European Union 7th Framework Programme (FP7/2007–2013) under grant agreement no. 603502 (EU project DACCIWA: Dynamics–aerosol–chemistry–cloud interactions in West Africa). We thank Mikhail Zhizhin from Earth Observation Group (EOG) of NOAA for providing us with the extracted flaring information from the VNF product. We are grateful to Godsgift Ezaina Umukoro (Department of Mechanical Engineering, University of Ibadan, Nigeria) for the kind support during the implementation of their combustion reaction theory into our parameterization.

The article processing charges for this open-access publication were covered by a Research Centre of the Helmholtz Association.

Edited by: A. Lauer
Reviewed by: C. Elvidge, M. Zhizhin, and one anonymous referee

References

API: Pressure-relieving and Depressuring Systems, ANSI/API STANDARD 521 FIFTH EDITION, JANUARY 2007, ISO 23251 (Identical), Petroleum and natural gas industries – Pressure-relieving and depressuring systems, American Petroleum Institute, Section 7.3.2.4: Design details h), 127, 2007.

Bader, A., Baukal, C. E., Bussman, W., and Zink, J.: Selecting the proper flare systems, American Institute of Chemical Engineers (AIChE), available at: http://people.clarkson.edu/wwilcox/Design/FlareSel.pdf (last access: October 2014), 2011.

CDIAC: Global CO_2 Emissions from Fossil-Fuel Burning, Cement Manufacture, and gas Flaring: 1751-2008, Carbon Dioxide Information Analysis Center (CDIAC), available at: http://cdiac.ornl.gov/ftp/ndp030/global.1751_2008.ems (last access: December 2015), 2015a.

CDIAC: National CO_2 Emissions from Fossil-Fuel Burning, Cement Manufacture, and gas Flaring: 1751-2011, Carbon Dioxide Information Analysis Center (CDIAC), Fossil-Fuel CO_2 Emissions by Nation, available at: http://cdiac.ornl.gov/ftp/ndp030/nation.1751_2011.ems (last access: December 2015), 2015b.

CM SAF: Operational Products: CFC – Fractional cloud cover instantaneous data (MSG disk, CM SAF definition), Version 350, available at: https://wui.cmsaf.eu/safira/action/viewPeriodEntry?id=11495_14063_15657_15672_16574_19152_20532_21207 (last access: November 2015), 2015.

Deetz, K. and Vogel, B.: Gas flaring emission estimation parameterization v2, available at: doi:10.5281/zenodo.61151, 2016.

Doumbia, T., Granier, L., Liousse, C., Granier, C., Rosset, R., Oda, T., and Fen Chi, H.: Analysis of fifty year Gas flaring Emissions from oil/gas companies in Africa, AGU Fall Meeting 2014, Dec 2014, San Francisco, United States, A13E-3217, 2014.

Dung, E. J., Bombom, L. S., and Agusomu, T. D.: The effects of gas flaring on crops in the Niger Delta, Nigeria, GeoJournal, 73, 297–305, 2008.

ECCAD: Emissions of atmospheric compounds & compilation of ancillary data (ECCAD), available at: http://eccad.sedoo.fr/eccad_extract_interface/JSF/page_critere.jsf (last access: December 2015), 2015.

EDGAR: Global Emissions EDGAR v4.3 FT2012, European Commission, Joint Research Centre (JRC)/PBL Netherlands Environmental Assessment Agency, Emission Database for Global Atmospheric Research (EDGAR), release version 4.3, available at: http://edgar.jrc.ec.europa.eu/, 2015 forthcoming, http://edgar.jrc.ec.europa.eu/overview.php?v=CO2ts1990-2014 (last access: December 2015), 2014.

EDGAR: Global Emissions EDGAR v4.3.2, European Commission, Joint Research Centre (JRC)/PBL Netherlands Environmental Assessment Agency, Emission Database for Global Atmospheric Research (EDGAR), release version 4.3.2, available at: http://edgar.jrc.ec.europa.eu/ (last access: December 2015), 2016.

EIA: CO_2 from the Consumption and Flaring of Natural Gas, International Energy Statistics, U.S. Energy Information Administration (EIA), available at: http://www.eia.gov/cfapps/ipdbproject/iedindex3.cfm?tid=90&pid=3&aid=8&cid=&syid=2010&eyid=2013&unit=MMTCD (last access: December 2015), 2015.

Ekpoh, I. J. and Obia, A. E.: The role of gas flaring in the rapid corrosion of zinc roofs in the Niger Delta Region of Nigeria, Environmentalist, 30, 347–352, 2010.

Elvidge, C. D., Baugh K. E., Kihn, E. A., Kroehl, H. W., and Davis, E. R.: Mapping city lights with nighttime data from the DMSP operation linescan system, Photogrammetric Engineering & Remote Sensing, 63, 727–744, 1997.

Elvidge, C. D., Ziskin, D., Baugh, K. E., Tuttle, B. T., Gosh, T., Pack, D. W., Erwin, E. H., and Zhizhin, M.: A fifteen year record of global natural gas flaring derived from satellite data, Energies, 2, 595–622, 2009.

Elvidge, C. D., Zhizhin, M., Hsu, F.-C., and Baugh, K. E.: VIIRS Nightfire: Satellite Pyrometry at Night, Remote Sens., 5, 4423–4449, 2013.

Elvidge, C. D., Zhizhin, M., Baugh, K., Hsu, F.-C., and Gosh, T.: Methods for Global Survey of Natural Gas Flaring from Visi-

ble Infrared Imaging Radiometer Suite Data, Energies, 9, 1–15, 2015.

Elvidge, C. D., Zhizhin, M., Baugh, K., Hsu, F.-C., and Ghosh, T.: Methods for Global Survey of Natural Gas Flaring from Visible Infrared Imaging Radiometer Suite Data, Energies 2016, 9, 14, doi:10.3390/en9010014, 2016.

EPA: Evaluation of the efficiency of industrial flares: Flare head design and gas composition, Research and Development, United States Environmental Protection Agency (EPA), EPA-600/2-85-106, Tab. 2–6, 1985.

Google Earth: Image 2014 DigitalGlobe, available at: https://earth.google.de/, 2014.

Guigard, S. E., Kindzierski, W. B., and Harper, N.: Heat Radiation from Flares. Report prepared for Science and Technology Branch, Alberta Environment, ISBN 0-7785-1188-X, Edmonton, Alberta, 2000.

Ismail, O. S. and Umukoro, G. E.: Modelling combustion reactions for gas flaring and its resulting emissions, Journal of King Saud University – Engineering Sciences, 28, 130–140, 2014.

Johnson, M. R., Devillers, R. W., and Thomson, K. A.: Quantitative Field Measurements of Soot Emission from Large Gas Flare using Sky-LOSA, Environ. Sci. Technol., 45, 345–350, 2011.

Knippertz, P., Evans, M. J., Field, P. R., Fink, A. H., Liousse, C., and Marsham, J. H.: The possible role of local air pollution in climate change in West Africa, Nature Climate Change, V5, 815–822, 2015.

Mirador: AIRS/Aqua Level 2 Standard physical retrieval (AIRS+AMSU), Total cloud fraction (CldFrcTot), https://mirador.gsfc.nasa.gov/collections/AIRX2RET__005.shtml (last access: April 2016), 2016.

NASA: Visible Infrared Imaging Radiometer Suite (VIIRS), available at: http://npp.gsfc.nasa.gov/viirs.html (last access: January 2016), 2016.

Nwankwo, C. N. and Ogagarue, D. O.: Effects of gas flaring on surface and ground waters in Delta State Nigeria, Journal of Geology and Mining Research, 3, 131–136, 2011.

Nwaugo, V. O., Onyeagba, R. A., and Nwahcukwu, N. C.: Effect of gas flaring on soil microbial spectrum in parts of Niger Delta area of southern Nigeria, African Journal of Biotechnology, 5, 1824–1826, 2006.

Osuji, L. C. and Avwiri, G. O.: Flared Gas and Other Pollutants Associated with Air quality in industrial Areas of Nigeria: An Overview, Chem. Biodivers., 2, 1277–1289, 2005.

R Core Team: R: A Language and Environment for Statistical Computing, R Foundation for Statistical Computing, Vienna, Austria, available at: http://www.R-project.org/ (last access: August 2016), 2013.

Sonibare, J. A. and Akeredolu, F. A.: A theoretical prediction of non-methane gaseous emissions from natural gas combustion, Energy Policy, 32, 1653–1665, 2004.

Strosher, M. T.: Investigations of flare gas emissions in Alberta, Final Report to: Environment Canada, Conservation and protection, the Alberta Energy and Utilities Board, and the Canadian Association of Petroleum Producers; Environmental Technologies, Alberta Research Council, Calgary, Alberta, 1996.

Strosher, M. T.: Characterization of Emissions from Diffuse Flare Systems, J. Air Waste Manage. Assoc., 50, 1723–1733, 2000.

van der Linden, R., Fink, A. H., and Redl, R.: Satellite-based climatology of low-level continental clouds in southern West Africa during the summer monsoon season, J. Geophys. Res.-Atmos., 120, 1186–1201, 2015.

VDI 3782: Dispersion of Air Pollutants in the Atmosphere, Determination of Plume rise, Verein Deutscher Ingenieure, VDI-Richtlinien 3782 Part 3, Equation 24, https://www.vdi.de/richtlinie/vdi_3782_blatt_3-ausbreitung_von_luftverunreinigungen_in_der_atmosphaere_berechnung_der_abgasfahnenueberhoehung/ (last access: October 2016), 1985.

VIIRS: VIIRS Nightfire (Nighttime Detection and Characterization of Combustion Sources), available at: http://ngdc.noaa.gov/eog/viirs/download_viirs_fire.html (last access: August 2016), 2015a.

VIIRS: VIIRS Nightfire (Flares Only Version), available at: http://ngdc.noaa.gov/eog/viirs/download_viirs_flares_only.html (last access: July 2015), 2015b.

Vogel, B., Vogel, H., Bäumer, D., Bangert, M., Lundgren, K., Rinke, R., and Stanelle, T.: The comprehensive model system COSMO-ART – Radiative impact of aerosol on the state of the atmosphere on the regional scale, Atmos. Chem. Phys., 9, 8661–8680, doi:10.5194/acp-9-8661-2009, 2009.

Zhang, X., Scheving, B., Shoghli, B., Zygarlicke, C., and Wocken, C.: Quantifying Gas Flaring CH_4 Consumption Using VIIRS, Remote Sens., 7, 9529–9541, 2015.